

<https://doi.org/10.1038/s42003-021-01815-w>

OPEN

Entropy-driven binding of gut bacterial β -glucuronidase inhibitors ameliorates irinotecan-induced toxicity

Hsien-Ya Lin ^{1,2,7}, Chia-Yu Chen ^{1,2,7}, Ting-Chien Lin^{1,2,7}, Lun-Fu Yeh¹, Wei-Che Hsieh¹, Shijay Gao¹, Pierre-Alain Burnouf³, Bing-Mae Chen³, Tung-Ju Hsieh¹, Punsaldulam Dashnyam¹, Yen-Hsi Kuo¹, Zhijay Tu ¹, Steve R. Roffler ^{3,4}✉ & Chun-Hung Lin ^{1,2,5,6}✉

Irinotecan inhibits cell proliferation and thus is used for the primary treatment of colorectal cancer. Metabolism of irinotecan involves incorporation of β -glucuronic acid to facilitate excretion. During transit of the glucuronidated product through the gastrointestinal tract, an induced upregulation of gut microbial β -glucuronidase (GUS) activity may cause severe diarrhea and thus force many patients to stop treatment. We herein report the development of uronic isofagomine (UIFG) derivatives that act as general, potent inhibitors of bacterial GUSs, especially those of *Escherichia coli* and *Clostridium perfringens*. The best inhibitor, C6-nonyl UIFG, is 23,300-fold more selective for *E. coli* GUS than for human GUS ($K_i = 0.0045$ and $105 \mu\text{M}$, respectively). Structural evidence indicated that the loss of coordinated water molecules, with the consequent increase in entropy, contributes to the high affinity and selectivity for bacterial GUSs. The inhibitors also effectively reduced irinotecan-induced diarrhea in mice without damaging intestinal epithelial cells.

¹Institute of Biological Chemistry, Academia Sinica, Taipei, Taiwan. ²Department of Chemistry, National Taiwan University, Taipei, Taiwan. ³Institute of Biomedical Sciences, Academia Sinica, Taipei, Taiwan. ⁴Graduate Institute of Medicine, College of Medicine, Kaohsiung Medical University, Kaohsiung, Taiwan. ⁵Institute of Biochemical Sciences, National Taiwan University, Taipei, Taiwan. ⁶The Genomics Research Center, Academia Sinica, Taipei, Taiwan. ⁷These authors contributed equally: Hsien-Ya Lin, Chia-Yu Chen, Ting-Chien Lin. ✉email: sroff@ibms.sinica.edu.tw; chunhung@gate.sinica.edu.tw

Colorectal cancer is the third most common cancer worldwide¹. More than half of colorectal cancer patients are diagnosed at stage 2 or later and therefore must receive chemotherapy. Irinotecan is the first-line chemotherapeutic agent for treatment of metastatic colorectal cancer^{2–4}, and SN-38 is its active metabolite that blocks DNA replication by inhibiting type I topoisomerase, leading to cell death^{5,6}. SN-38 is converted to SN-38-glucuronide by UDP-glucuronosyltransferase in the liver to facilitate drug excretion. However, microflora-encoding β -glucuronidases (GUSs) are notorious for reversing the glucuronidation to release SN-38 in the intestinal lumen and thus represent the major cause of undesirable effects. Among patients taking irinotecan, 87% suffer from severe delayed diarrhea^{7–9}, and ~10% become dehydrated, whereas ~3.5% are at high risk of death owing to neutropenia^{10,11}.

Glucuronidation is one of the most common biological conjugation reactions^{12–14}. The monosaccharide glucuronic acid can be attached to an oxygen, nitrogen, or sulfur atom of substrates, catalyzed by UDP-glucuronosyltransferases, rendering the resulting metabolites easily excreted via urine or bile¹⁵. However, intestinal bacterial GUSs cleave the attached glucuronic acid for use as a carbon source, allowing potentially toxic compounds to re-enter the enterohepatic circulation^{16,17}. Furthermore, several food-derived toxic compounds are released back into the bloodstream by these GUSs, such as amygdalin (found in apricots, peaches, bitter almonds, plums)¹⁸, 2-amino-3-methylimidazo[4,5-f]quinoline (genotoxic/carcinogenic compound formed in meat and fish during cooking)¹⁹, and bis(2-ethylhexyl)phthalate and its derivatives (plasticizers)¹². These toxic compounds can promote tumor formation^{20,21}, although they can be metabolized by UDP-glucuronosyltransferase to produce harmless glucuronide conjugates.

Several approaches have been proposed to suppress the irinotecan-induced intestinal toxicity, including enhanced the delivery of SN-38 to tumor²², adjusted the releasing rate of SN-38²³, and reduced the immune response^{24,25}. Another promising approach was to develop specific inhibitor of intestinal bacterial GUSs^{9,26,27}. Redinbo and coworkers were the first to report a selective inhibitor (ASN03273363) for gut bacterial GUSs ($K_i = 0.16 \mu\text{M}$ for *Escherichia coli* GUS, *EcGUS*) that does not inhibit human GUS (*HsGUS*). ASN03273363 can alleviate the undesirable effects caused by SN-38⁹. The *HsGUS* and *EcGUS* structures differ in loop 3, which is one of eight loops near the active site. Loop 3 of *EcGUS* has 23 residues, 17 more than that of *HsGUS* and interacts with ASN03273363 through hydrophobic contacts, explaining the potency and selectivity of ASN03273363. Despite its potency, ASN03273363 has one therapeutic drawback, namely that more than half of the microbial homologs have a loop 3 of <15 residues (Supplementary Fig. 1) and thus cannot interact with this inhibitor²⁸. Moreover, the loop 3 sequence differs substantially among the various bacterial GUSs.

Uronic isofagomine (UIFG, **1**) potently inhibits both mammalian and bacterial GUSs, owing to ionic interactions between the protonated ring nitrogen and the two catalytic glutamates²⁹. Notably, we found that the incorporation of an alkyl substituent to UIFG could affect the binding affinity with different GUSs. To understand the underlying structural basis, we prepared C6-propyl, -hexyl, and -nonyl UIFGs (**2–4**, respectively) and resolved the eight X-ray crystal structures of **1–4** bound to *EcGUS* or *Bifidobacterium dentium* GUS (*BdGUS*). C6-alkylation expelled the water molecules in the GUS active site, suggesting that the corresponding entropy increase contributes to the enhanced selectivity ($K_i = 4.5 \text{ nM}$ for *EcGUS* vs. $105 \mu\text{M}$ for *HsGUS*, a difference of 23,300-fold). To demonstrate *in vivo* efficacy, the inhibitors were tested for cytotoxicity and their ability to inhibit bacterial GUSs in the mouse intestine. The results indicated that

C6-alkyl UIFG derivatives hold great promise for therapeutic intervention.

Results

Synthesis of inhibitors 2–4. GUS contains a deep enzyme active site (the two catalytic glutamates lie ~12 Å below the protein surface). To determine whether additional interactions with drugs could be achieved, we introduced three alkyl substituents (propyl, hexyl, nonyl) to C6 of UIFG (**2–4**, see Fig. 1a for the structures). The synthesis began with inexpensive D-arabinose (Fig. 1b). Alcohol **6** was prepared at large scale (>10 g) in seven steps with 54% overall yield following a procedure modified from Stick et al.³⁰. The triflate, obtained by treating compound **6** with triflic anhydride in pyridine, was further converted into the cyanide **7** using KCN as the nucleophile in the presence of 18-crown-6 (82% yield in two steps). The nucleophilic addition of *n*-C₃H₇MgCl in diethyl ether to **7**, followed by NaBH₄-mediated reduction, gave the corresponding amine **8** (39% yield in two steps) with exclusive stereoselectivity (S-configuration for the newly formed stereogenic center)^{30,31}. The perfect stereoselectivity was realized owing to the coordination of the magnesium (of the Grignard reagent) with the ring oxygen of **7**³¹.

In a similar manner, amines **9** and **10** were obtained as single isomers at 54% and 49% yield, respectively. However, the next-step reductive amination failed to reach a satisfying yield when compounds **8–10** were subjected to hydrogenation by following the condition from our previous study (in the presence of conc. HCl over 20% Pd(OH)₂ on charcoal at 50 psi H₂)²⁹. Thin-layer chromatography (TLC) analysis indicated that the reaction bottleneck was the formation of the cyclic imine. The reduction was achieved when the hydrogenation process was performed in a continuous flow chemistry system (Vapourtec[®]) by well-controlled circulation of amines **8–10** and 100 psi H₂ through pre-coated 20% Pd(OH)₂/C. The desired substituted isofagomines **11–13** were obtained in high yield (78–82%). The final products **2–4** were obtained with total yield of 27–73% in three steps by *N*-Cbz protection, selective oxidation of the primary alcohol, and removal of Cbz by hydrogenation. Notably, the selective oxidation of the methyl hydroxyl group was the key step, avoiding our previous use of tedious protection and deprotection steps²⁹. The selective oxidation of the primary alcohol could be achieved in moderate yield (38–78%) by bubbling oxygen through a mixture of 10% Pt/C and *N*-Cbz-protected isofagomines **11–13** under basic conditions in H₂O/isopropanol/acetone (Fig. 1b).

Inhibition of GUSs by UIFG (1) and its derivatives (2–4).

Among the eight loops near the catalytic site of bacterial GUSs, loops 3–5 have highly variable sequences, which underlie substrate preferences of the GUSs^{32,33}. Especially, loops 3 and 4 often differ in length³³. To examine if the synthesized inhibitors displayed any specificity for different GUSs, we prepared the GUSs from four different bacterial strains belonging to major phyla of the gut microbiota, including *EcGUS*, *BdGUS*, *Clostridium perfringens* GUS (*CpGUS*), and *Lactobacillus gasseri* GUS (*LgGUS*). *E. coli* and *C. perfringens* are opportunistic bacteria, whereas *B. dentium* and *L. gasseri* are commensal bacteria. Notably, *EcGUS*, *CpGUS*, and *LgGUS* contain a longer loop 3 (>15 residues), whereas *HsGUS* and *BdGUS* both have only six residues in their loop 3. In addition, loop 4 of *BdGUS* is five residues longer than that of the other GUSs (Supplementary Fig. 2). Comparison of sequences from different bacterial GUSs helped us to understand if the potency of GUS inhibition correlated with loop length, as well as their preference for xenobiotic glucuronides. We previously reported that the structures and conformations of loops 3 and 5 are closely linked to substrate preference³².

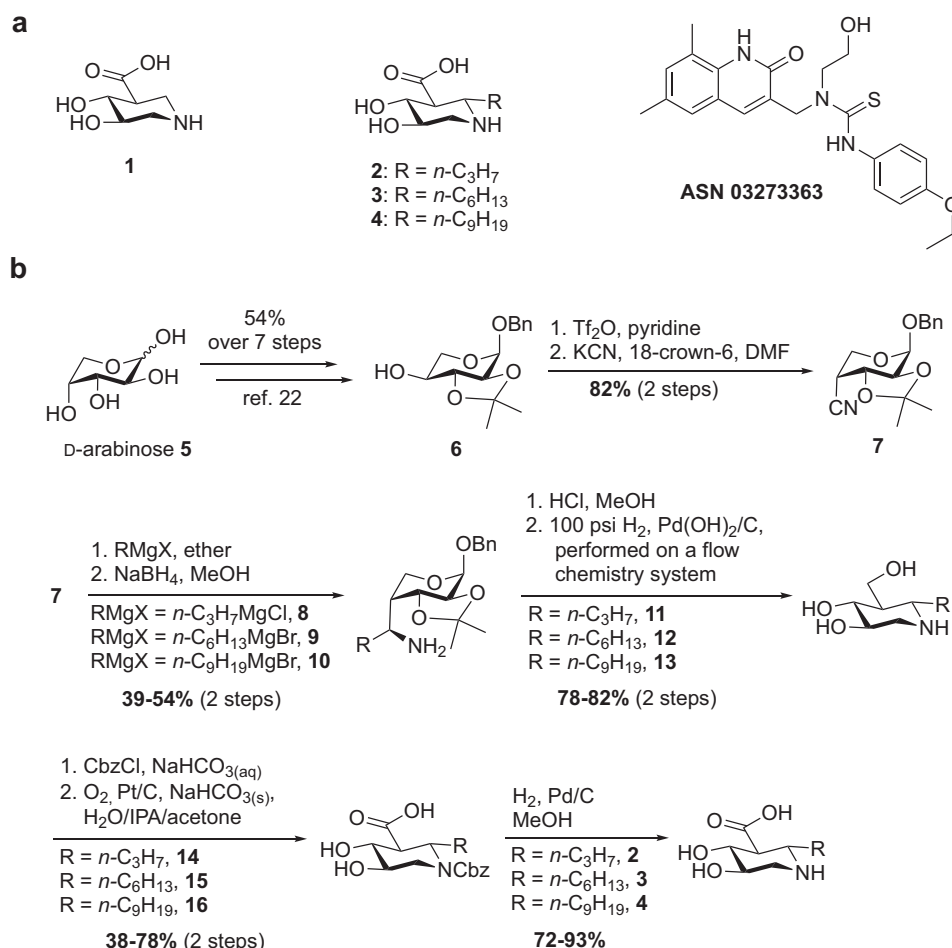


Fig. 1 Molecular structures of inhibitors and synthetic scheme for UIFG derivatives. **a** Molecular structures of UIFG (**1**) and its C6-alkylated derivatives **2-4** and ASN03273363. **b** Synthesis of **2-4** and substituted isofagomines **11-13**.

Table 1 Inhibition constants for UIFGs (**1**) and derivatives (**2-4**) for *HsGUS* and four gut bacterial GUSs.

Enzyme	K_i (μM)				
	1	2	3	4	ASN03273363
<i>HsGUS</i>	0.18 \pm 0.002	36.1 \pm 7.5	5.3 \pm 0.9	105.2 \pm 4.8	NI ^a
<i>EcGUS</i>	0.016 \pm 0.002	0.035 \pm 0.009	0.003 \pm 0.0006	0.0045 \pm 0.0007	0.16 ^a
<i>CpGUS</i>	0.0065 \pm 0.0012	0.62 \pm 0.041	0.17 \pm 0.066	0.026 \pm 0.0073	0.97 ^a
<i>LgGUS</i>	0.11 \pm 0.033	18.8 \pm 3.92	0.86 \pm 0.18	0.27 \pm 0.074	NI
<i>BdGUS</i>	0.0074 \pm 0.002	4.9 \pm 1.2	0.86 \pm 0.2	0.44 \pm 0.02	NI

NI no inhibition.
^aRef. 20.

Table 1 lists the inhibition constants for inhibitors **1-4** for the five GUSs. Inhibitor **1** appeared to be potent for both human and bacterial GUSs (e.g., K_i = 180 nM for *HsGUS*, 16 nM for *EcGUS*, 7.4 nM for *BdGUS*, 6.5 nM for *CpGUS*). Surprisingly, the C6-substituted UIFG contributed to differential selectivity between bacterial and *HsGUS*: the longer the C6-alkyl chain, the more potent the inhibition of microbial GUSs. Particularly, C6-nonyl UIFG (**4**) had 23,300-fold higher potency for *EcGUS* than for *HsGUS* (K_i = 4.5 nM for *EcGUS* vs. 105 μM for *HsGUS*). Though less potent for *LgGUS* and *BdGUS*, **4** still inhibited these two GUSs in the sub-micromolar range (K_i = 270 and 440 nM, respectively) and was selective for the two bacterial GUSs (390- and 240-fold more potent than for *HsGUS*, respectively).

Likewise, C6-hexyl UIFG (**3**) also was 1770-fold more potent for inhibiting *EcGUS* than *HsGUS*.

Table 1 also illustrates a notable trend. In comparison with **1**, the introduction of an alkyl chain indeed decreased affinity for all GUSs, yet there was a trend of increasing affinity with longer chain length. This compensation effect was more important for the inhibition of *EcGUS* and *CpGUS*. To help explain these intriguing observations, we relied on the structures of inhibitor-bound *EcGUS* and *BdGUS*. Additionally, we also examined the inhibition of isofagomines **11-13** that are the analogs of **2-4**, respectively. The main difference is that **11-13** contain a hydroxymethyl group at C5, instead of a carboxylic acid. Despite a much lower level of inhibition for **11-13** (IC_{50} = 272.3, 24.9,

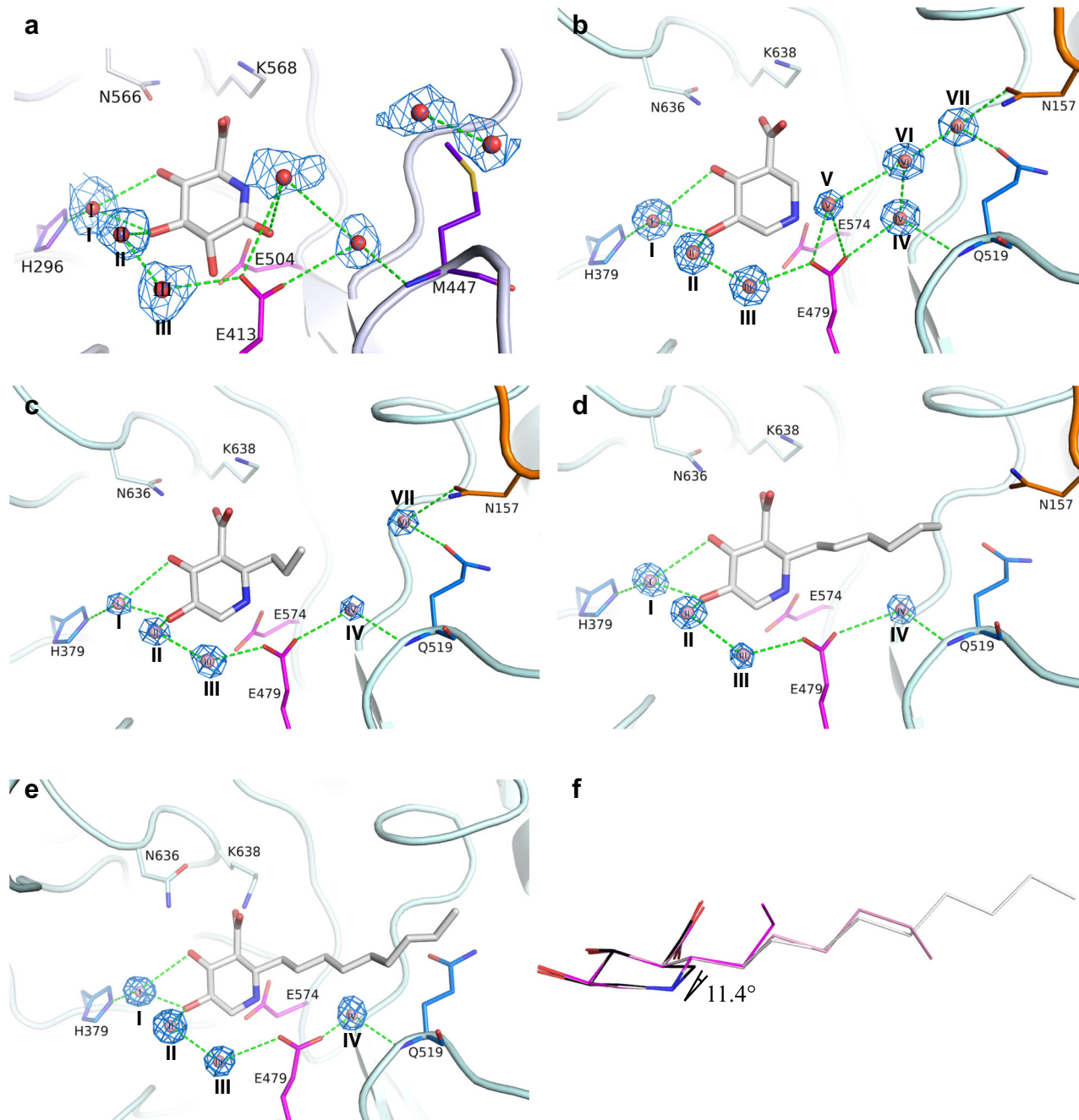


Fig. 2 Crystal structures of inhibitors bound to *BdGUS*. **a** A water-mediated H-bond network within the substrate binding site of *EcGUS* in complex with glucaro- δ -lactam and **b-e** *BdGUS* in complex with inhibitors **1-4**. The interactions were similar between the sugar moiety and *BdGUS*. The $2F_o - F_c$ density maps of water molecules are colored blue. The alkyl substituents of **2-4** appear to expel some of the water molecules. **f** Superimposition of inhibitors **1-4** in the crystal structures. C6 of **2-4** deviates 11.4° from that of **1**.

and 3.6 μ M for *EcGUS*, respectively), these compounds displayed a consistent trend observed for inhibitors **2-4**, i.e., a longer alkyl chain could improve the inhibition of *EcGUS*. This trend was reversed, however, for *HsGUS*: the percentage of inhibition = 4.5%, 0.6%, and -0.5% for **11-13** at 1 mM ($IC_{50} > 1$ mM), respectively.

The alkyl chain of **2-4 disrupts the water-mediated hydrogen-bond network at the inhibitor binding site.** To resolve the details of the binding interactions, we determined the complete structures for inhibitors **1-4** bound to *EcGUS* and *BdGUS*,

(Fig. 2b-e and Supplementary Fig. 3). These structures displayed binding interactions similar to those with the UIFG moiety, which is equivalent to glucuronic acid (the reaction product). For *BdGUS*, the two catalytic residues Glu479 and Glu574 (equivalent to Glu413 and Glu504 in *EcGUS* that correspond to the acid/base and nucleophile, respectively) formed ionic interactions with the endocyclic amine of UIFG²⁹. Asn636 and Lys638, characterized as a unique conserved N-K motif in loop 8³³, provided hydrogen bonds (H-bonds) and electrostatic interactions, respectively, with the C5-carboxylate of inhibitors **1-4** (Fig. 2b-e). The other conserved residues were categorized into two groups depending on whether they formed direct or indirect H-bonds with the

hydroxyl groups of the bound inhibitor. The former group (including Arg632, Asp179, and Tyr543) interacted directly with the C5-carboxylate and C4-hydroxyl groups of the inhibitors, whereas the latter (His379, His413, and Asn478) formed water-mediated H-bonds with the C3-OH and Glu574. Additionally, Trp619 provided a hydrophobic contact (Supplementary Fig. 4) with one face of the iminocyclitol ring. Because the resolutions of the four structures for *BdGUS* (1.7–2.4 Å) were higher than those for *EcGUS* (2.5–3.2 Å), water molecules could be visualized in the catalytic site. Seven highly coordinated water molecules (I–VII) clustered in the active site of *BdGUS*/1 and formed an H-bond network with the inhibitor. Water molecules I–III were conserved in all of the *BdGUS* structures and located near the UIFG-binding moiety to mediate interactions between the inhibitor and certain residues. In contrast, molecules VI–VII were located near the aglycone-binding moiety.

As compared with the inhibitor 1-bound form, two water molecules (V and VI) were not present in the structure of 2-bound *BdGUS*, likely owing to the presence of the propyl substituent of 2. Interestingly, waters V–VII were absent in the inhibitors 3- and 4-bound forms. Although water molecules were ambiguous in the active site of *EcGUS* (apo form) owing to the limited resolution, in the glucaro- δ -lactam-bound structure of *EcGUS* (PDB code: 3K4D)⁹, we indeed observed five water molecules that also formed an H-bond network similar to what was observed in the inhibitor-bound structures of *BdGUS* (Fig. 2a, b).

Isothermal titration calorimetry was used to measure the thermodynamics of the binding of 1 or 2 to *EcGUS* and *BdGUS* (Fig. 3a, Supplementary Table 1, and Supplementary Fig. 5). The potent inhibition of 1 was contributed mainly by enthalpy ($\Delta H = -10.47$ and -9.12 kcal mol⁻¹ for *BdGUS* and *EcGUS*, respectively). At pH 8.0, the endocyclic amine of inhibitor 2 (pKa = 9.4) was mostly protonated, which afforded a stronger electrostatic interaction with catalytic residues than did 1 (pKa = 8.0)²¹. The results for 2 were quite different. In addition to a small negative enthalpy change (about -2 to -4 kcal mol⁻¹), binding was contributed mainly by entropy ($+4.6$ kcal mol⁻¹ for *BdGUS* in Tris buffer; $+7.1$ and $+5.0$ kcal mol⁻¹ for *EcGUS* in Tris and phosphate buffer, respectively). With the aforementioned structural information, the differences between the thermodynamic parameters for 1 and 2 support the idea that the lack of H-bonded water molecules for 2 diminished the coordinated H-bond network, which disfavored binding and thus the observed enthalpy penalty ($\Delta\Delta H_{1-2} = +8.5$ kcal mol⁻¹ for *BdGUS* in Tris buffer; $+6.2$ and $+5.5$ kcal mol⁻¹ for *EcGUS* in Tris and phosphate buffer, respectively). Furthermore, the expulsion of water molecules also correlated with the entropy increase (i.e., $-T\Delta\Delta S_{1-2} = -6.2$ kcal mol⁻¹ for *BdGUS* in Tris buffer; -5.6 and -4.6 kcal mol⁻¹ for *EcGUS* in Tris and phosphate buffer, respectively). Therefore, introduction of an alkyl substituent to C6 of UIFG produced entropy-driven binding. Further titration studies of the hexyl- and nonyl-substituted UIFGs (3 and 4) became impossible because the enthalpy change was close to zero in Tris buffer. It is known that protonation by Tris in solution makes the total process highly exothermic³⁴; however, it may interfere with proton transfer in the binding reaction of inhibitor and GUS. Instead of Tris buffer, the use of phosphate buffer allowed measurement of the thermodynamic parameters. Similar to the previous trend, the entropy contribution of 3 and 4 increased with the length of alkyl chain ($-T\Delta\Delta S_{2-3} = -1.32$ kcal mol⁻¹ and $-T\Delta\Delta S_{2-4} = -1.34$ kcal mol⁻¹ for *EcGUS*), while the enthalpy contribution decreased ($\Delta\Delta H_{2-3} = +0.04$ kcal mol⁻¹ and $\Delta\Delta H_{2-4} = +0.99$ kcal mol⁻¹ for *EcGUS*). These results explain why the incorporation of an alkyl chain to C6 of UIFG reduced the binding affinity, but chain elongation increased the entropy

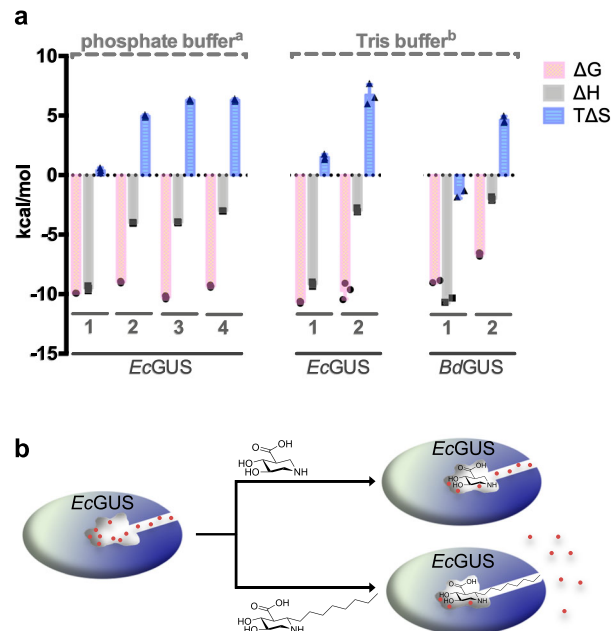


Fig. 3 Entropy-driven binding of inhibitors 1-4 with *EcGUS* and *BdGUS*.

a Graphical presentation to show the thermodynamic parameters of the binding interactions of *EcGUS* and *BdGUS* in complex with inhibitors 1-4 at 298 K. The detailed analysis is shown in Supplementary Table 1. ^a 250 mM NaCl, 20 mM KH₂PO₄, 100 mM Na₂HPO₄, pH 8.0. ^b 250 mM NaCl, 20 mM Tris, pH 8.0. **b** Cartoon presentation to demonstrate that several water molecules (represented by red circles) are orderly located at the active site of gut bacterial GUSs, as shown in *EcGUS* (the left model), and can be displaced by binding with UIFGs. The best inhibitor, C6-nonyl UIFG, displays tight binding with *EcGUS* ($K_i = 4.5$ nM) and 23,300-fold higher selectivity for *EcGUS* than for human GUS (the bottom right). GUSs are mainly different in the aglycone-binding site, which can be leveraged to develop selective inhibitors. If UIFGs have no substitution (the top right), selective inhibition no longer exists.

contribution, thereby improving binding (Fig. 3b). Therefore, the water-mediated H-bond network likely plays an important role in both substrate/inhibitor binding to bacterial GUSs and their catalytic activity.

Water molecules were also reported in published structures of GUSs, such as *BdGUS* (apo form), *HsGUS* (apo form, PDB code: 3HN3), and *EcGUS* (bound with glucaro- δ -lactam, PDB code: 3K4D). Notably, several water molecules in the apo structures overlap with the hydroxyl and carboxyl groups of glucuronic acid, implying that the sugar-binding site either interacts with the complexed waters (apo form) or with the glucuronic acid moiety (binding site occupied by the substrate/inhibitor), as shown in Supplementary Fig. 6.

Furthermore, Phe448 in the 2-bound *EcGUS* structure was found to rotate $\sim 100^\circ$ toward the active site to form a hydrophobic interaction³⁵ with the propyl group (Supplementary Figs. 3e and 7), as compared to the same residue in 1-bound *EcGUS*. This change shortened the distance between the propyl group and the center of the phenyl ring of Phe448 by 1.4 Å, thus providing a better hydrophobic contact. Interestingly, owing to the longer alkyl chains of 3 and 4, Phe448 rotated outward in *EcGUS*/3 and *EcGUS*/4 and thus increased the hydrophobic contact area. This additional hydrophobic interaction might have compensated for the binding energy loss owing to the absence of the water-mediated H-bond network, leading to the observed lower K_i values of 2-4 for *EcGUS* compared with other GUSs. Furthermore, *EcGUS* contains a narrower aglycone-binding site

than *LgGUS* and *BdGUS* (Supplementary Fig. 8). The alkyl substituent of the inhibitors therefore facilitated an increase in hydrophobic contacts with nonpolar residues of loops 3 and 5 in *EcGUS*, e.g., such as Leu361, Phe365 in loop 3, and Val446, Met447, and Phe448 in loop 5.

Compounds 2–4 inhibit *EcGUS* without affecting the survival of *E. coli*. To examine if inhibitors 2–4 could inhibit GUS activity *in vivo*, *E. coli* cells ($OD_{600} = 1.89$) were treated with each of 2–4 for 30 min, after which GUS activity was measured. The IC_{50} was as follows: 2, 1.2 μ M; 3, 18.6 nM; and 4, 3.69 nM (Supplementary Fig. 9a). Consistent with the aforementioned K_i values, 4 was the most potent inhibitor. The fact that intracellular GUS activity could be inhibited indicated that 2–4 were, in fact, able to cross the cell membrane. Additionally, to evaluate cell viability, *E. coli* cultures were treated with ampicillin (positive control), DMSO, or inhibitors 2–4 (100 μ M) for 6 h. An agar-based colony-forming assay revealed that 2–4 did not significantly affect *E. coli* viability (Supplementary Fig. 9b).

Compound 3 inhibits the activity of intestinal microbial GUSs in BALB/c mice. We evaluated the potential cytotoxicity of 3 in cultures of non-cancerous human mammary epithelial cells (H184b5f5/M10) and human fibroblasts (GM637). The cells were chosen as representatives of the intestinal mucosa, the lumen of which is composed of epithelia and fibroblasts. Cells were incubated with 3 (0.001–100 μ M) for 24 h. No cytotoxicity was evident, even at 100 μ M of 3. In contrast, ASN03273363 at 100 μ M inhibited the proliferation of both cell types by >50% (Supplementary Fig. 10a).

We also investigated the potential toxicity of 3 to intestinal cells using female BALB/c mice (8–12 weeks old). The mice were given 3 (37.5 mg per kg body weight) or ASN03273363 (65 mg) via oral gavage for 5 days. The mice were then sacrificed and the intestines removed. Hematoxylin and eosin staining revealed that neither compound affected the health of the epithelial layer or the intestinal glandular structure (Supplementary Fig. 10b). In addition, we performed real-time *in vivo* gastrointestinal inhibition of bacterial GUSs using whole-body *in vivo* imaging (Fig. 4a and Supplementary Figs. 11, 12). The mice were gavaged in the same manner as described above. Following the final gavage, 500 μ g of FDGiCu (fluorescein-di- β -D-glucuronide as a non-fluorescent probe) was injected intravenously. Upon digestion by intestinal bacterial GUSs, FDGiCu is hydrolyzed to produce fluorescein (as the hydrolyzed product) that can be detected as fluorescence in the intestinal region. Reduced fluorescence was observed in mice fed with inhibitor 3, suggesting that 3 could effectively inhibit gut bacterial GUSs. Moreover, to examine whether inhibitor 3 can block SN-38-induced toxicity by irinotecan (CPT-11), a total of 32 mice were divided into four groups for this study, including vehicle control, inhibitor 3 only (5.8 μ g given orally twice per day), CPT-11 only (30 mg per kg intravenously daily), and CPT-11 with inhibitor 3 at the same doses as above. Mice were treated for 10 days. The results indicate that neither the negative control nor inhibitor 3 caused diarrhea in mice (Fig. 4b). The mice treated with CPT-11 developed diarrhea on day 7, until they reached a peak on day 11. In contrast, diarrhea was significantly suppressed when inhibitor 3 was given to mice receiving CPT-11.

Discussion

In general, gut bacterial GUSs mostly contain a hydrophobic aglycone-binding site. Although some bacterial GUSs indeed have substrate preference for hydrophilic aglycones, those GUSs are secreted extracellularly to degrade polysaccharide glucuronides³³.

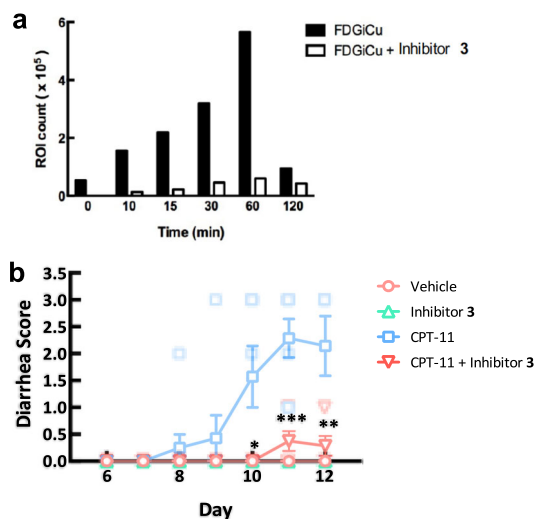


Fig. 4 Treatment with inhibitor 3 demonstrates inhibition of GUS and protection against diarrhea caused by CPT-11 damage in mice.

a Inhibition of GUS *in vivo*. Mice were given 3 via oral gavage. After 1 h, fluorescein-di- β -D-glucuronide (FDGiCu; 500 μ g in 100 μ L) was injected intravenously. The hydrolysis product (fluorescein) generated in the gut was quantified over a 2 h period by *in vivo* imaging (excitation 465 nm, emission 520 nm). The maximum fluorescein fluorescence was observed 60 min after injection of vehicle control. At 2 h post injection, most of the FDGiCu has been excreted and thus fluorescence is reduced. The region of interest (ROI) was analyzed with Living Image Software. **b** Effect of inhibitor 3 to protect against diarrhea caused by CPT-11. Diarrhea severity was scored as described in methods. Mice receiving CPT-11 (blue squares) experienced severe diarrhea from days 7–11, whereas mice receiving inhibitor 3 with CPT-11 (red triangles) displayed significantly reduced diarrhea (Welch's unpaired *t*-test, day 9, $p = 0.3632$; day 10, $*p = 0.0284$; day 11, $***p = 0.0005$; day 12, $**p = 0.0057$).

Because secreted GUSs are not xenotoxic, they were not the focus of our study. On the other hand, *HsGUS* is a lysosomal enzyme that degrades glucuronate-containing glycosaminoglycans; its aglycone-binding site is quite hydrophilic.

Taking the comparison between *EcGUS* and *HsGUS* as an example, the aglycone-binding site of *EcGUS* is surrounded by five hydrophobic residues, namely Phe365, Leu361, Val446, Met447, and Phe448, which are located in loops 3 and 5, whereas the site of *HsGUS* is surrounded by Ser485^{loop 5}, Tyr505^{loop 6}, His509^{loop 6}, and Thr599^{loop 8} (Supplementary Fig. 13a, b). This difference explains why substitution with an alkyl group at C6 of UIFG remarkably enhanced its binding affinity and selectivity for *EcGUS*.

Our observed entropy-driven binding of inhibitors 2–4 to bacterial GUSs is reminiscent of the iminoribitol-based hydroxypyrrolidines that inhibit human 5'-methylthioadenosine phosphorylase³⁶. Schramm and coworkers reported that the binding involves a favorable entropy of -17.6 kcal mol⁻¹ with unfavorable enthalpy of $+2.6$ kcal mol⁻¹. The binding to the phosphorylase results in substantial structural changes, including collapse of the enzyme active site and the expulsion of water from both the active site and subunit interfaces³⁶.

Moreover, because the aglycone-binding sites of *CpGUS* and *EcGUS* are very similar in terms of hydrophobicity and size, it is not surprising that 2–4 could potentially and selectively inhibit *CpGUS* (Supplementary Figs. 8a and 7b). However, *LgGUS* and *BdGUS* have more spacious aglycone-binding sites than *EcGUS* and *CpGUS* (Supplementary Fig. 8b, c), explaining why 2–4 did not have high affinity for *LgGUS* and *BdGUS*. To develop

inhibitors with higher affinity for *LgGUS* and *BdGUS*, a bulkier group should be considered, e.g., phenyl group. This also supports the idea that a functionalized substituent, such as an NH_2 -containing moiety, at C6 is essential for successful addition of any group at C6, depending on the features of the aglycone-binding site. Consequently, it is possible to develop potent and selective inhibitors for a particular type of GUS as long as the aglycone-binding site can be predicted in accordance with the sequences of loops 3–5.

In conclusion, we identified a water-mediated H-bond network in the catalytic site of bacterial GUSs. C6-substituted UIFGs were found to be entropy-favored inhibitors that achieved potent and selective inhibition of *EcGUS* and *CpGUS*, especially the enzymes produced by opportunistic and pathogenic bacteria that are major causes of xenobiotic toxicity. Moreover, the inhibitors we developed not only effectively inhibited gut bacterial GUSs in mice but also were not cytotoxic to the gut bacteria or intestinal epithelia. Because substituted iminocyclitols (such as Miglitol) are widely used for therapeutic intervention, our findings pave the way for iminocyclitols to be utilized in microbiota research and for clinical intervention.

Methods

Preparation of GUSs. *HsGUS* was prepared as described³⁷. Recombinant *EcGUS* was cloned into pET-28a (Novagen), and *CpGUS*, *LgGUS*, and *BdGUS* were cloned into pET-15b (Novagen). All proteins were overexpressed in *E. coli* BL21 (DE3) upon induction with 0.5 mM isopropyl β -D-1-thiogalactoside pyranoside for 24 h at 16 °C. Recombinant proteins were purified to homogeneity by Ni^{2+} -affinity and size-exclusion chromatography. Purified proteins were then stored in gel-filtration buffer (20 mM succinic acid pH 6.0, 150 mM NaCl for *BdGUS*; 20 mM Tris-HCl pH 8.0, 250 mM NaCl for *EcGUS*, *LgGUS*, and *CpGUS*) and concentrated to 20 mg mL^{-1} as determined by the Bradford method.

Measurement of IC_{50} and K_i values. GUS activities were determined by the hydrolysis rate of 4-methylumbelliferyl- β -glucuronide. Emission at 445 nm was monitored using an excitation wavelength of 365 nm to measure the release of fluorescent 4-methylumbelliferone at 37 °C. Enzyme kinetics were measured in 50 mM HEPES pH 7.5 for *BdGUS* and *EcGUS* and 50 mM sodium acetate pH 4.5 for *HsGUS*, *LgGUS*, and *CpGUS*. To measure K_i values, the activity assays were carried out in 100 μL of the aforementioned buffers containing 1 mM 4-methylumbelliferyl- β -glucuronide and varying concentrations of inhibitor. *BdGUS* (6.9 nM), *EcGUS* (2.5 nM), *LgGUS* (4.0 nM), *CpGUS* (3.8 nM), and *HsGUS* (7.5 nM) were used for the inhibition assays. The K_i values for inhibitors 1–4 and *HsGUS*, *LgGUS*, *CpGUS*, and *BdGUS* were verified by Lineweaver–Burk plot²⁹, and apparent K_M values were calculated. Plotting the apparent K_M values as a function of the inhibitor concentrations generated the secondary plot. K_i was determined by calculating the negative value of the resulting x intercept. As previously reported, the progression curves for inhibitors 1–4 and *EcGUS* revealed time-dependent inhibition^{29,38}, and K_i values were determined by the following simple reversible slow-binding equation:



$$P = V_s \times t + (V_0 - V_s) \frac{(1 - e^{-kt})}{k_{\text{obs}}} \quad (2)$$

where V_0 and V_s are the initial and steady-state rates, respectively, k_{obs} is the apparent rate constant for the steady state, and P is the amount of product that accumulates during a period of time t .

$$k_{\text{obs}} = k_3[I] + k_4 \quad (3)$$

The k_{obs} values were plotted as a function of inhibitor concentration. The linear fit of the data provided the kinetic rate constants k_3 and k_4 , and then the apparent K_i was calculated from the ratio of k_4/k_3 .

Crystallization and data collection. Crystals of *EcGUS* and *BdGUS* were grown at room temperature (298 K) using the hanging-drop vapor diffusion method. The crystallization conditions were as follows: 20 mg mL^{-1} *EcGUS* in 2 μL of 0.2 M MgCl_2 , 0.1 M Tris-HCl, pH 8.5, 21% (w/v) PEG 4K; 5 mg mL^{-1} *BdGUS* in 2 μL of 0.1 M sodium cacodylate, pH 6.5, 8% (w/v) PEG 20K. Crystals of inhibitor/*BdGUS* and inhibitor/*EcGUS* were obtained by soaking. First, compounds 1–4 were dissolved in 100% DMSO to a concentration of 20 mM. For ligand soaking, crystals were transferred into the reservoir solution containing a compound concentration

of 5 mM, incubating for 5 min prior to cryocooling. After 5 min, the crystals were transferred into reservoir solution containing 20% glycerol as a cryoprotector. The crystals were then flash-frozen in liquid nitrogen and stored for data collection. Table 2 summarizes the data statistics.

Determination and refinement of the crystal structures. The crystal structures of all complexes were solved by molecular replacement with PHENIX AutoMR using the published *EcGUS* apo structure as the starting search model (PDB entry 3K46). Modeling was performed with PHENIX AutoBuild. Structures underwent multiple rounds of manual rebuilding and refinement with Coot and PHENIX. The figures were generated in Pymol.

Isothermal titration calorimetry. *BdGUS* and *EcGUS* were diluted to appropriate concentrations in dialysis buffer (20 mM Tris-HCl pH 8.0, 250 mM NaCl or 20 mM KH_2PO_4 , 100 mM Na_2HPO_4 , pH 8.0, 250 mM NaCl). All samples were passed through 0.22 μm filters (Millipore). Isothermal titration calorimetry was performed using the Auto-ITC200 (MicroCal, Northampton, MA) at 298 K. Inhibitors 1–4 were dissolved in a stock solution of DMSO. To avoid heating effects owing to different concentrations of DMSO in the syringe and protein solutions, 5% DMSO was added to the protein. Curve fitting of the experimental data was performed with Origin version 7.0 (MicroCal).

Cells and animals. H184B5F5/M10 non-cancerous human mammary epithelial cells and GM637 non-cancerous human fibroblasts were obtained from the American Type Culture Collection (ATCC, Manassas, VA). The cells were cultured in RPMI supplemented with 10% bovine calf serum, 2.98 g L^{-1} HEPES, and 2 g L^{-1} NaHCO_3 in a 5% CO_2 humidified atmosphere at 37 °C. Female BALB/c mice (8–12 weeks old) were purchased from the National Laboratory Animal Center (Taipei, Taiwan). All animals were allowed free access to food and water, and experiments were done according to the standards of the United Kingdom Coordinating Committee on Cancer Research Guidelines for the Welfare of Animals in Experimental Neoplasia. All animal experiments were certified by Institute Animal Care and Use committee of Academia Sinica (ASACUC), protocol ID: 12-07-384.

In vitro cytotoxicity. To study the potential cytotoxicity of inhibitor 3 to normal cells, 10,000 cells per well were seeded in a 96-well plate and incubated at 37 °C overnight. The cells were then incubated with a graded concentration of 3 for 24 h, washed twice with sterile phosphate buffered saline, and incubated for 16 h in fresh medium containing 1 μCi [^3H]thymidine per well. The cells were trypsinized and harvested on glass fiber filters, radioactivity was counted, and % inhibition was calculated as: [c.p.m. (sample) \times 100/c.p.m. (control)].

Colon histology. Mice were given an inhibitor (11.75 nmol in 100 μL) via oral gavage twice a day for 5 days. After the final gavage, the mice were sacrificed and the colon harvested and fixed in neutral buffered formalin. Colon samples were embedded in paraffin and stained with hematoxylin and eosin.

In vivo imaging of GUS activity. Female BALB/c mice (8–12 weeks old) were given various amounts of an inhibitor via oral gavage 1 h before imaging. Following the final gavage, 500 μg of FDG-Cu (Invitrogen) was injected intravenously. The intensity of hydrolyzed fluorescein was assessed by in vivo imaging system (Caliper Life Sciences) and quantified as GUS activity.

In vivo diarrhea test. Irinotecan (CPT-11) was purchased from Sigma as a hydrochloride salt. For animal studies, CPT-11 was dissolved in double-distilled water as a stock solution (2.5 mg mL^{-1}). The inhibitor 3 was dissolved in 100% DMSO (5.78 mg mL^{-1}), then diluted with double-distilled water to 57.8 μg mL^{-1} . Vehicle control mice received an equivalent volume of 1% DMSO in double-distilled water as the experimental groups. Thirty-two healthy female BALB/c mice (6–8 weeks old) were divided into four groups of eight mice each: (I) vehicle control group, animals receiving 250 μL of double-distilled water intraperitoneally (i.p.) and 100 μL of 1% DMSO solution by oral gavage twice per day; (II) inhibitor 3 group, 250 μL of double-distilled water i.p. and inhibitor 3 (100 μL) by oral gavage twice per day (10 h separation) starting on day-1; (III) CPT-11 group in which CPT-11 (30 mg kg^{-1}) was injected i.p. once in the morning with oral gavage of vehicle control twice for 10 days, and (IV) CPT-11 + inhibitor 3 group in which CPT-11 (30 mg kg^{-1}) was injected i.p. once in the morning for 10 days and inhibitor 3 (100 μL) was orally gavaged twice per day (10 h separation). Total injected volume was considered as equal for each mouse and all mice were carefully monitored. The degree of diarrhea was monitored daily and described by using a scoring system defined as: 0, normal stool; 1, slight perianal staining of the coat; 2, moderate perianal staining of the coat; 3, watery mucosal-infused stool with severe perianal staining of the coat.

Table 2 Summary of crystal structure determination and refinement.

PDB code	BdGUS				
	Apo form 6LD6	Inhibitor 1 6LDB	Inhibitor 2 6LDD	Inhibitor 3 6LDO	Inhibitor 4 6LDC
<i>Data collection</i>					
Space group	P2 ₁	P2 ₁	P2 ₁	P2 ₁	P2 ₁
Cell dimensions <i>a, b, c</i> (Å)	92.583, 104.902, 160.62	92.69, 104.64, 160.504	92.606, 105.928, 161.89	92.645, 104.77, 161.044	93.142, 104.814, 160.819
α, β, γ (°)	90, 91.16, 90	90, 91.29, 90	90, 91.33, 90	90, 91.22, 90	90, 91.08, 90
Resolution (Å)	29.6–2.204 (2.283–2.204)	24.85–1.651 (1.71–1.651)	29.59–2.449 (2.536–2.449)	26.6–1.881 (1.948–1.881)	27.84–2.175 (2.253–2.175)
R_{sym} or R_{merge}	0.086 (0.385)	0.054 (0.418)	0.088 (0.471)	0.089 (0.513)	0.055 (0.189)
$I / \sigma I$	18.9 (4.3)	22.0 (3.8)	14.8 (2.9)	20.1 (2.5)	23.8 (5.7)
Completeness (%)	98.9 (90.3)	93.8 (90.4)	93.14 (46.62)	92.33 (60.9)	97.08 (77.86)
Redundancy	4.3 (4.0)	3.4 (3.4)	3.7 (3.8)	3.4 (4.2)	4.1 (2.9)
<i>Refinement</i>					
Resolution (Å)	29.6–2.204 (2.283–2.204)	24.85–1.651 (1.71–1.651)	29.59–2.449 (2.536–2.449)	26.6–1.881 (1.948–1.881)	27.84–2.175 (2.253–2.175)
No. reflections	154377	343510	155860	241740	160237
$R_{\text{work}} / R_{\text{free}}$	0.1519/0.1991	0.1555/0.1825	0.1443/0.2056	0.1419/0.1747	0.1426/0.1912
No. atoms					
Protein	19636	19660	19636	19636	19552
Ligand/ion	0	44	56	68	80
Water	1935	2689	1949	1608	2030
<i>B</i> -factors					
Protein	22.80	21.31	23.60	27.70	21.20
Ligand/ion	22.10	19.91	23.50	26.40	20.20
Water	30.00	20.00	25.70	35.10	24.50
R.m.s. deviations					
Bond lengths (Å)	0.008	0.015	0.008	0.007	0.007
Bond angles (°)	1.11	1.36	1.14	1.10	1.06
Ramachandran favored (%)	97	97	96	97	97
Ramachandran outliers (%)	0	0.041	0.12	0	0.042
PDB code	EcGUS				
	Inhibitor 1 6LEG	Inhibitor 2 6LEJ	Inhibitor 3 6LEL	Inhibitor 4 6LEM	
<i>Data collection</i>					
Space group	C2	C2	C2	C2	
Cell dimensions <i>a, b, c</i> (Å)	207.527, 75.926, 168.281	167.686, 76.551, 125.426	165.781, 76.72, 124.888	68.361, 76.404, 126.4	
α, β, γ (°)	90, 96.79, 90	90, 124.85, 90	90, 124.636, 90	90, 124.966, 90	
Resolution (Å)	29.79–2.603 (2.696–2.603)	29.75–2.617 (2.711–2.617)	29.47–2.498 (2.588–2.498)	28.25–3.188 (3.302–3.188)	
R_{sym} or R_{merge}	0.179 (0.897)	0.092 (0.642)	0.111 (0.763)	0.172 (0.953)	
$I / \sigma I$	13.3 (1.5)	17.8 (2.0)	15.7 (1.6)	9.7 (1.1)	
Completeness (%)	99.2 (94.7)	97.9 (89.1)	97.9 (90.3)	98.4 (91.2)	
Redundancy	3.4 (3.4)	5.3 (4.6)	3.6 (2.8)	6.0 (2.9)	
<i>Refinement</i>					
Resolution (Å)	29.79–2.603 (2.696–2.603)	29.75–2.617 (2.711–2.617)	29.47–2.498 (2.588–2.498)	28.25–3.188 (3.302–3.188)	
No. reflections	79253	61283	43895	21727	
$R_{\text{work}} / R_{\text{free}}$	0.2317/0.2877	0.2367/0.2795	0.2378/0.2868	0.2108/0.2695	
No. atoms					
Protein	19223	9507	9521	9446	
Ligand/ion	44	28	34	40	
Water	231	65	125	0	
<i>B</i> -factors					
Protein	51.32	57.16	58.33	77.73	
Ligand/ion	51.54	57.36	58.74	77.75	
Water	30.99	36.81	32.28	71.98	
R.m.s. deviations					
Bond lengths (Å)	0.008	0.012	0.013	0.003	
Bond angles (°)	1.04	1.53	1.64	0.66	
Ramachandran favored (%)	93	92	93	90	
Ramachandran outliers (%)	0.97	0.77	0.94	1.12	

Statistics and reproducibility. No data were excluded from the analyses. Unless otherwise noted, all graphs depict mean \pm SEM. Statistical significance was determined with Welch's unpaired *t*-test. Biostatistical analyses were done with GraphPad software (GraphPad Prism 7, La Jolla, CA, USA).

Reporting summary. Further information on research design is available in the Nature Research Reporting Summary linked to this article.

Data availability

The data that support the findings of this study are available from the corresponding author on reasonable request. All the data supporting the findings of this study are available in the Supplementary Information. The source data underlying Table 1 and Fig. 4b are provide as Supplementary Data 1 and 2. The coordinates of the crystal structures have been deposited to PDB and the entry numbers are 6LD6 (apo BdgUS), 6LDB (BdgUS/1), 6LDD (BdgUS/2), 6LDO (BdgUS/3), 6LDC (BdgUS/4), 6LEG (EcGUS/1), 6LEJ (EcGUS/2), 6LEL (EcGUS/3), and 6LEM (EcGUS/4).

Received: 19 October 2020; Accepted: 8 February 2021;

Published online: 04 March 2021

References

- Miller, K. D. et al. Cancer treatment and survivorship statistics. *CA Cancer J. Clin.* **66**, 271–289 (2016).
- Foubert, F., Matysiak-Budnik, T. & Toucheffeu, Y. Options for metastatic colorectal cancer beyond the second line of treatment. *Dig. Liver Dis.* **46**, 105–112 (2014).
- Bailly, C. Irinotecan: 25 years of cancer treatment. *Pharmacol. Res.* **148**, 104398–104409 (2019).
- de Man, F. M., Goey, A. K. L., van Schaik, R. H. N., Mathijssen, R. H. J. & Bins, S. Individualization of irinotecan treatment: a review of pharmacokinetics, pharmacodynamics, and pharmacogenetics. *Clin. Pharmacokinet.* **57**, 1229–1254 (2018).
- Staker, B. L. et al. The mechanism of topoisomerase I poisoning by a camptothecin analog. *Proc. Natl Acad. Sci. USA* **99**, 15387–15392 (2002).
- Pommier, Y. Topoisomerase I inhibitors: camptothecins and beyond. *Nat. Rev. Cancer* **6**, 789–802 (2006).
- Armand, J. P. CPT-11: clinical experience in phase I studies. *Semin. Oncol.* **23**, 27–33 (1996).
- Kaneda, N. & Yokokura, T. Nonlinear pharmacokinetics of CPT-11 in rats. *Cancer Res.* **50**, 1721–1725 (1990).
- Wallace, B. D. et al. Alleviating cancer drug toxicity by inhibiting a bacterial enzyme. *Science* **330**, 831–835 (2010).
- Rothenberg, M. L., Meropol, N. J., Poplin, E. A., Van Cutsem, E. & Wadler, S. Mortality associated with irinotecan plus bolus fluorouracil/leucovorin: summary findings of an independent panel. *J. Clin. Oncol.* **19**, 3801–3807 (2001).
- Benson, A. B. 3rd et al. Recommended guidelines for the treatment of cancer treatment-induced diarrhea. *J. Clin. Oncol.* **22**, 2918–2926 (2004).
- Croom, E. Metabolism of xenobiotics of human environments. *Prog. Mol. Biol. Transl. Sci.* **112**, 31–88 (2012).
- Tephly, T. R. & Burchell, B. UDP-glucuronosyltransferases: a family of detoxifying enzymes. *Trends Pharmacol. Sci.* **11**, 276–279 (1990).
- Geraud, F. & Paris, A. Glucuronidation: a dual control. *Gen. Pharmacol.* **31**, 683–688 (1998).
- Burchell, B. & Stevenson, I. Developmental, genetic and environmental aspects of drug biotransformation and conjugation - introduction. *Biochem. Soc. Trans.* **12**, 1–1 (1984).
- Lu, K., Mahbub, R. & Fox, J. G. Xenobiotics: interaction with the intestinal microflora. *ILAR J.* **56**, 218–227 (2015).
- Carmody, R. N. & Turnbaugh, P. J. Host-microbial interactions in the metabolism of therapeutic and diet-derived xenobiotics. *J. Clin. Invest.* **124**, 4173–4181 (2014).
- Newton, G. W., Schmidt, E. S., Lewis, J. P., Conn, E. & Lawrence, R. Amygdalin toxicity studies in rats predict chronic cyanide poisoning in humans. *West. J. Med.* **134**, 97–103 (1981).
- Humblot, C. et al. β -Glucuronidase in human intestinal microbiota is necessary for the colonic genotoxicity of the food-borne carcinogen 2-amino-3-methylimidazo[4,5-f]quinoline in rats. *Carcinogenesis* **28**, 2419–2425 (2007).
- Kim, D. H. & Jin, Y. H. Intestinal bacterial β -glucuronidase activity of patients with colon cancer. *Arch. Pharm.* **24**, 564–567 (2001).
- Dabek, M., McCrae, S. I., Stevens, V. J., Duncan, S. H. & Louis, P. Distribution of β -glucosidase and β -glucuronidase activity and of β -glucuronidase gene gus in human colonic bacteria. *FEMS Microbiol. Ecol.* **66**, 487–495 (2008).

- Sharkey, R. M. et al. Enhanced delivery of SN-38 to human tumor xenografts with an anti-Trop-2-SN-38 antibody conjugate (sacituzumab govitecan). *Clin. Cancer Res.* **21**, 5131–5138 (2015).
- Rustin, G. et al. A multicenter, open-label, expanded phase 2 study to evaluate the safety and efficacy of etirinotecan pegol, a polymer conjugate of irinotecan, in women with recurrent platinum-resistant or refractory ovarian cancer. *Gynecol. Oncol.* **147**, 276–282 (2017).
- Hedigan, K. Herbal medicine reduces chemotherapy toxicity. *Nat. Rev. Drug Discov.* **9**, 765–765 (2010).
- Zhang, X. et al. Darunavir alleviates irinotecan-induced intestinal toxicity in vivo. *Eur. J. Pharmacol.* **834**, 288–294 (2018).
- Cheng, K. W. et al. Pharmacological inhibition of bacterial β -glucuronidase prevents irinotecan-induced diarrhea without impairing its antitumor efficacy in vivo. *Pharmacol. Res.* **139**, 41–49 (2019).
- Chen, Z. et al. Identify old drugs as selective bacterial β -GUS inhibitors by structural-based virtual screening and bio-evaluations. *Chem. Biol. Drug Des.* **95**, 368–379 (2020).
- Wallace, B. D. et al. Structure and inhibition of microbiome β -glucuronidases essential to the alleviation of cancer drug toxicity. *Chem. Biol.* **22**, 1238–1249 (2015).
- Dashnyam, P. et al. Substituent location position of iminocyclitols determines the potency and selectivity for xenobiotic-reactivating enzymes. *J. Med. Chem.* **63**, 4617–4627 (2020).
- Goddard-Borger, E. D. & Stick, R. V. An expeditious synthesis of isofagomine. *Aust. J. Chem.* **60**, 211–213 (2007).
- Zhu, X., Sheth, K. A., Li, S., Chang, H. H. & Fan, J. Q. Rational design and synthesis of highly potent β -glucocerebrosidase inhibitors. *Angew. Chem. Int. Ed. Engl.* **44**, 7450–7453 (2005).
- Dashnyam, P. et al. β -Glucuronidases of opportunistic bacteria are the major contributors to xenobiotic-induced toxicity in the gut. *Sci. Rep.* **8**, 16372 (2018).
- Pollet, R. M. et al. An atlas of β -glucuronidases in the human intestinal microbiome. *Structure* **25**, 967–977 (2017).
- Hill, J. O. & Wadso, I. Some thermochemical properties of N, N, N-triacetylammonia. *Acta Chem. Scand.* **22**, 1590–1594 (1968).
- Deza, M. M. & Deza, E. *Encyclopedia of Distances* 438 (Springer, 2013).
- Guan, R. et al. Entropy-driven binding of picomolar transition state analogue inhibitors to human 5'-methylthioadenosine phosphorylase. *Biochemistry* **50**, 10408–10417 (2011).
- Bernt, K. M. et al. Enzyme-activated prodrug therapy enhances tumor-specific replication of adenovirus vectors. *Cancer Res.* **62**, 6089–6098 (2002).
- Pellock, S. J. et al. Gut microbial β -glucuronidase inhibition via catalytic cycle interception. *ACS Cent. Sci.* **4**, 868–879 (2018).

Acknowledgements

This work was supported by the Summit Project at Academia Sinica (AS-SUMMIT-109 and AS-KPQ-109-BioMed) and the Ministry of Science and Technology (MOST-108-3114-Y-001-002), Taiwan. We thank Drs. Chris Jao and Meng-Ru Ho of the Biophysics Core Facility for technical assistance with the thermodynamics experiments, Ms. Hui-Ling Shi of the National Core Facility for protein crystallization screening, and the beamlines of the National Synchrotron Radiation Research Center (Taiwan) for X-ray diffraction and data collection.

Author contributions

H.-Y.L., C.-Y.C., and T.-C.L. contributed equally to this work. H.-Y.L., C.-Y.C., Z.T., and C.-H.L. organized and wrote the manuscript. T.-C.L. performed the kinetic and bacterial cell survival experiments. C.-Y.C., L.-F.Y., W.-C.H., and S.G. synthesized all the inhibitors. H.-Y.L., T.-J.H., P.D., and Y.-H.K. re-solved the crystal structures. H.-Y.L. carried out the thermodynamics analysis. P.-A.B., B.-M.C., and S.R.R. contributed to the in vivo GUS activity and diarrhea assays and in vitro cytotoxicity assays.

Competing interests

The authors declare no competing interests.

Additional information

Supplementary information The online version contains supplementary material available at <https://doi.org/10.1038/s42003-021-01815-w>.

Correspondence and requests for materials should be addressed to S.R.R. or C.-H.L.

Reprints and permission information is available at <http://www.nature.com/reprints>

Publisher's note Springer Nature remains neutral with regard to jurisdictional claims in published maps and institutional affiliations.



Open Access This article is licensed under a Creative Commons Attribution 4.0 International License, which permits use, sharing, adaptation, distribution and reproduction in any medium or format, as long as you give appropriate credit to the original author(s) and the source, provide a link to the Creative Commons license, and indicate if changes were made. The images or other third party material in this article are included in the article's Creative Commons license, unless indicated otherwise in a credit line to the material. If material is not included in the article's Creative Commons license and your intended use is not permitted by statutory regulation or exceeds the permitted use, you will need to obtain permission directly from the copyright holder. To view a copy of this license, visit <http://creativecommons.org/licenses/by/4.0/>.

© The Author(s) 2021